Low-frequency, low-degree solar p-mode properties from 22 years of birmingham solar oscillations network data

Davies, Guy; Broomhall, A. M.; Chaplin, W. J.; Elsworth, Y.; Hale, Steven

DOI:
10.1093/mnras/stu080

Monthly Notices
of the
ROYAL ASTRONOMICAL SOCIETY

MNRAS **439,** 2025–2032 (2014)
Advance Access publication 2014 February 7

doi:10.1093/mnras/stu080

Low-frequency, low-degree solar p-mode properties from 22 years of Birmingham Solar Oscillations Network data

G. R. Davies,[1⋆] A. M. Broomhall,[1,2,3] W. J. Chaplin,[1] Y. Elsworth[1] and S. J. Hale[1]

[1]*HiROS/BiSON, University of Birmingham, Edgbaston, Birmingham B15 2TT, UK*
[2]*Institute of Advanced Study, University of Warwick, Coventry CV4 7HS, UK*
[3]*Centre for Fusion, Space, and Astrophysics, Department of Physics, University of Warwick, Coventry CV4 7AL, UK*

Accepted 2014 January 13. Received 2014 January 6; in original form 2013 September 5

ABSTRACT

The solar low-degree low-frequency modes of oscillation are of particular interest as their frequencies can be measured with very high precision and hence provide good constraints on seismic models. Here we detect and characterize these valuable measures of the solar interior from a 22 yr Birmingham Solar Oscillations Network data set. We report mode frequencies, line widths, heights, amplitudes, and rotational splitting, all with robust uncertainties. The new values of frequency, rotational splitting, amplitude, and line width we provide will help place new constraints on hydrostatic and rotational structure, plus diagnostics of near-surface convection. Further to this, by assuming simple power laws, we extrapolate mode properties to lower frequencies. We demonstrate that the low-l low-frequency p modes have a low signal-to-noise ratio and that this cannot be overcome simply by continued observation. It will be necessary to observe the Sun in novel ways to 'beat' the intrinsic granulation noise.

Key words: methods: data analysis – Sun: helioseismology – Sun: oscillations.

1 INTRODUCTION

One of the major observational challenges of modern low angular degree (l) helioseismology is the detection of modes of oscillation below 1 mHz (Chaplin et al. 2003). Key to these detections is very long temporal-baseline observations with low noise characteristics and good duty cycles. With over 20 yr of high quality, high duty-cycle Birmingham Solar Oscillations Network (BiSON) observations, now is the time to re-examine the low-frequency region of the solar oscillation spectrum.

We can use the properties of the low-degree solar acoustic (p) and gravity (g) modes to constrain the conditions throughout the Sun including its deep interior. While controversy surrounds the claimed observations of g modes (García et al. 2007; Appourchaux et al. 2010), detection of low-frequency p modes ($\leq$1.3 mHz) is possible with very long data sets (Chaplin et al. 2001; Garcia et al. 2001; Broomhall et al. 2007). Observationally we find that acoustic mode lifetime is a function of frequency. Below around 2 mHz lifetime increases as frequency decreases. The long mode lifetimes observed at low frequency produce very narrow peaks in frequency in the spectra of long time series, which allows mode frequencies to be determined with high accuracy and precision (Chaplin et al. 2002). However, the additional constraint on solar structure and dynamics provided by low-frequency p modes does not come easily. With decreasing frequency (decreasing radial order n), the upper turning point of the acoustic cavity occurs at increasing depth in and below the solar photosphere, so there is a greater distance between the mode cavity and the energy source in the very outer layers of the Sun. In addition to decreasing signal strength at lower frequency, the magnitude of the solar noise in radial velocity measurements (primarily due to granulation) increases at lower frequency. Put simply, the signal-to-noise ratio of low-frequency modes is poor.

The detection of low-frequency p modes in the low signal-to-noise regime provides a challenge that has led helioseismologists to develop robust methods of analysis. Typically one asks 'is the observed peak or structure a genuine signal or a result of noise?' Both frequentist (Broomhall et al. 2007) and Bayesian (Broomhall et al. 2010; Appourchaux 2011) approaches have been applied to estimate the probability that a peak is due to noise (the H0 null hypothesis) or that some observed structure is a mode of oscillation (the H1 hypothesis). Given some detection threshold, a peak is typically classified as either a mode candidate or just noise. Mode candidates that present characteristics that are consistent with expectations (guided by both patterns in existing observations and results from modelling) may be elevated to detections.

Further information can be extracted from the observed signatures of modes in the power spectrum; for example: the line width, amplitude, and rotational splitting. Acoustic modes of oscillation are stochastically excited and intrinsically damped by broad-band noise generated near the top of the convective zone. By analogy with a damped harmonic oscillator, the mode shape expected in the

⋆ E-mail: grd349@gmail.com

frequency domain is a Lorentzian. The mode line width is proportional to the inverse of the mode lifetime, revealing information on the time-scale of the damping (Chaplin et al. 1998). Furthermore, the mode amplitude is sensitive to the mode lifetime and to the rate of convective energy input, giving insight into the convective process (Houdek et al. 1999). Finally non-radial modes, modes with degree (l) greater than zero, have their degeneracy lifted by rotation, thus revealing the dynamical solar interior (Thompson et al. 2003).

Here we present parameters of the low-degree low-frequency solar p modes from an analysis of data collected by the BiSON between 1991 January and 2012 December. In Section 2 we detail the data preparation and analysis procedures to identify and parametrize modes. The detections are contained in Section 3 along with results of regression analyses to fit the mode line width and amplitude as a function of frequency. Using the determined relationships we demonstrate the extent of the challenge of improving our knowledge of solar modes of oscillation at low frequency. Finally, we draw our conclusions in Section 4.

2 ANALYSIS

We use the data collected using resonance scattering spectrometers (RSS; Brookes, Isaak & van der Raay 1978) of the six station BiSON (Elsworth et al. 1995). BiSON RSS compare the Doppler shifted solar 769.9 nm K D1 absorption line to a reference line in the laboratory frame. These shifts are measured as variations in resonant scattered intensity which are calibrated into radial velocities each day for each of the six stations. Using these data, a time series is built based on a routine that attempts to maximize the signal-to-noise ratio in the low-frequency region (0.8–1.3 mHz). Here we use 40-s cadence BiSON data selecting a start date of 1991 January 01 and running to 2012 December 31. We do not use the BiSON data back as far as the beginning of the network in 1978 as it was not until early 1991 that the network consisted of 5, and later in the year 6, reliably working stations providing high duty cycles. As detailed analysis is run in the frequency domain the time series is converted to a frequency power spectrum. We have developed tools specifically to improve the signal-to-noise ratio in the low-frequency regime and will devote some time here to detailing the procedures and decisions made.

2.1 Data preparation

2.1.1 Daily calibration

The daily calibration procedure is based around that of Elsworth et al. (1995) which uses the large variations in observed radial velocity due to the Earth's rotation and orbit to calibrate the relatively small radial velocities caused by to the Sun. To improve the noise characteristics of the data set we apply the correction for terrestrial atmospheric differential extinction of Davies (in preparation). Differential extinction across the solar disc introduces low-frequency drifts at the extreme ends of the observational day. By modelling and correcting for these drifts one realizes large improvements in the noise characteristics at low frequency. The addition of this correction improves the low-frequency signal-to-noise ratio by up to 25 per cent primarily by removing the otherwise present large discontinuities in the time series that appear at early morning and late evening for each station. In addition to reducing noise, this correction allows for the acceptance of more data at the extremes of each day thereby increasing the final duty cycle.

2.1.2 Time series construction

After daily calibration, we are left with six time series of varying noise levels, one from each observation site that must be combined to produce a final time series. In the best case scenario as many as four sites observe contemporaneously (i.e. at the same time), and in the worst case bad weather will preclude observations from any site. Here we detail a procedure to combine data from all stations to produce a single time series observation optimized for the best signal-to-noise ratio at low frequency.

Assembling BiSON data to maximize low-frequency signal-to-noise ratio is a balancing act between getting a high duty cycle in the time series and a low noise level in the power spectrum low-frequency band. Once the data have been collected and calibrated, the only decision required is whether or not to include a subset of the data in the final time series. Including only the best data produces the lowest noise levels but the drop in duty cycle severely impacts the signal levels. Including all data gives the best duty cycle but results in a high noise level. Clearly a compromise is required.

The BiSON low-frequency time series construction procedure sets a noise threshold (q) above which subsections of data are rejected and below which they are accepted. The metric we use to assess the noise level is the mean power of the 0.8–1.3 mHz frequency range, since the power in that frequency range is primarily noise. A somewhat arbitrary choice is made to individually assess subsections defined by the boundaries of overlaps between different stations. In the case of contemporaneous data, only the subsection with the lowest noise parameter is accepted in accordance with the findings of Chaplin et al. (1997a).

In the following section we define a proxy for the signal-to-noise ratio which is to be maximized by varying the noise threshold in the data assembly procedure.

2.1.3 The relation between duty cycle and signal

The observational duty cycle impacts the magnitude of a signal in an observed power spectrum because power leaks from the signal into the background. The effect of missing data in a time series on its spectrum is characterized by the window function and it affects the observed amplitude of the signal. Given an uninterrupted signal $s(t)$, or $S(\nu)$, modified by some observation window $w(t)$, or $W(\nu)$, the resulting power spectrum $P(\nu)$, scaled to match variance and total power, is the convolution of the signal and window in the frequency domain (Lazrek & Hill 1993):

$$P(\nu) = S(\nu)W(\nu). \tag{1}$$

With this we can define duty-cycle efficiency, $\eta(q,\ \nu_0)$, with the noise threshold, q, defined in Section 2.1.2, as the strength of signal observed in the power spectrum divided by the strength of the original signal measured at the underlying frequency of the signal, ν_0,

$$\eta(q,\ \nu_0) = \frac{P(\nu_0)}{S(\nu_0)} = \frac{S(\nu_0)W_q(\nu_0)}{S(\nu_0)}, \tag{2}$$

where the choice of q leads to a given $W_q(\nu)$.

Modes of oscillation in the low-frequency regime are expected to have long lifetimes and hence narrow line widths (a few frequency bins in a 22 yr observation). If we assume our signal $S(\nu)$ to be very narrow, that we approximate by a delta function, the resulting $P(\nu)$ will be the window function itself. Then the height of the window function at ν_0, $W(\nu_0)$, will be a measure of the duty cycle

efficiency, i.e.

$$\eta(q, \nu_0) \approx W_q(\nu_0). \quad (3)$$

The noise threshold (q) for a subsection of data does not linearly correspond to the measured noise level in the power spectrum generated from the full data set. The noise level across the previously defined frequency band in the full 22 yr spectrum ($Q_{\rm full}$) is a combination of the noise seen in each subset and the noise from combining different subsets, typically introduced by low-frequency offsets that vary for each station. We have tested a number of values for q and have chosen the data set which maximizes the ratio of the duty-cycle efficiency to the low-frequency noise in the full power spectrum, i.e. $\eta(q, \nu_0)/Q_{\rm full}$. This results in a best data set for $q = 35\,{\rm m^2\,s^{-2}\,Hz^{-1}}$ with statistics for the duty-cycle efficiency of 68.3 per cent and full time series noise level of $Q_{\rm full} = 52.6\,{\rm m^2\,s^{-2}\,Hz^{-1}}$.

2.1.4 The power spectrum

Having selected the optimum time series we convert to the frequency domain using a fast Fourier transform (FFT) and produce a power spectrum scaled as power per Hz. Low signal-to-noise ratio peaks are more visible if the power spectrum is displayed as the signal-to-noise ratio. This conversion is achieved by simply dividing the power spectrum by the local background function which is determined using a very wide (130 μHz) box-car smooth. The signal-to-noise ratio in the region of interest is displayed in Fig. 1.

Fig. 1 gives us an indication of the signal present in the data but we can do better with a more quantitative approach. In the absence of a signal, a signal-to-noise ratio spectrum would have a mean value of unity with a χ^2_2 noise distribution. With this information we can determine the probability of observing a given signal-to-noise ratio, i.e. we can apply an H0 test. Here we apply the H0 test specified in Appourchaux et al. (2012) where the test is considered over a frequency width of half the width of the large spacing (the average frequency distance between consecutive $l = 0$ modes).

Furthermore, we can apply the test to signal-to-noise ratio spectra with different levels of re-binning applied. This takes advantage of the knowledge that modes in the low-frequency region, although narrow, are distributed over a number of frequency bins (the bin width of the original power spectrum is 1.44 nHz). The signal-to-noise ratio spectrum, box-car re-binned over N bins has a χ^2_{2N} noise distribution. Fig. 2 shows a graphical representation of the results

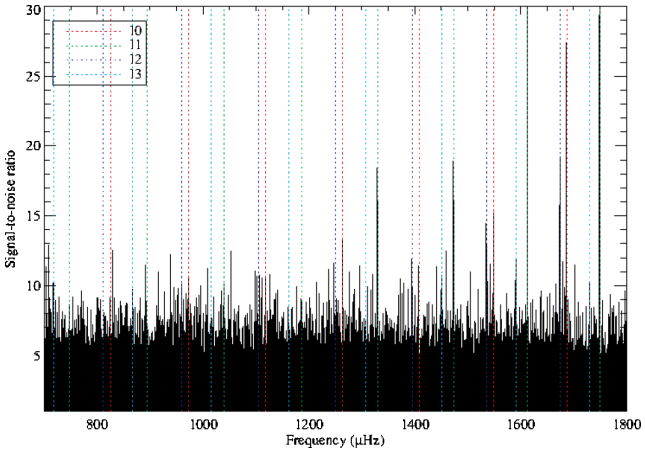

Figure 1. Frequency signal-to-noise ratio spectrum from the optimum data preparation pipeline with modelled frequency predictions as vertical lines.

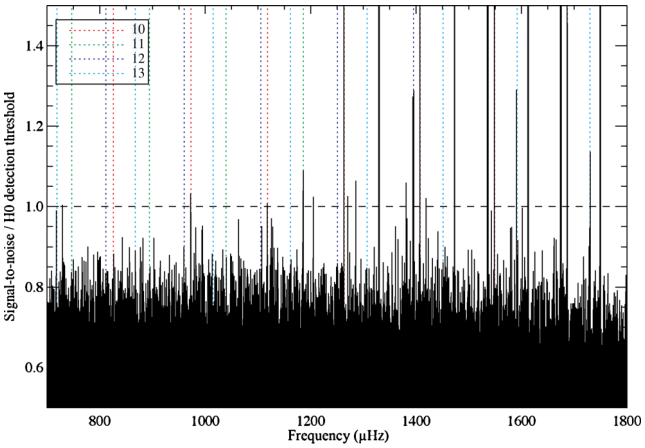

Figure 2. 50 individual re-binned spectra plotted on the same axes, with re-binning widths from 1 to 50 bins plotted as the signal-to-noise ratio and then divided by H0 detection threshold at the 1 per cent level. Points above 1.0 suggest the power is 'unlikely' to be a result of noise alone, although with 50 different spectra plotted some (≈8) false positives are to be expected. Modelled frequency predictions as shown as vertical lines.

from the H0 tests applied by displaying the signal-to-noise ratio normalized by the H0 detection threshold. In this way, plotting re-binned spectra allows peaks that fail the test to fall into the noise but peaks with significant power to show prominently.

In detail, Fig. 2 shows 50 individual signal-to-noise ratio spectra overplotted on the same axes. Each spectrum has been re-binned over a different width with values varying from $N = 1$ to 50 bin widths, and each spectrum has been normalized by the 1 per cent H0 detection threshold. We rebin up to 50 bin widths in increments of one as this is expected to produce around eight false positives in the whole plot. The plot range is 1.1 mHz and H0 is assessed over 67 μHz with a 1 per cent threshold. This makes the number of tests $50 \times 1100 / 67$, which will give the expectation value for the number of false positives when multiplied by the 0.01 threshold. Hence, we expect around eight false positives from a few hundred true positives. This allows us to say that peaks above the threshold of unity are relatively unlikely to be a result of the χ^2_{2N} degrees-of-freedom noise distribution. Hence, we have used a frequentist approach to demonstrate that there is structure in the low-frequency region of the power spectrum that is 'unlikely' to be a result of noise.

2.2 Bayesian mode detection

The frequentist H0 tests applied so far are sufficient to demonstrate that there is signal in the low-frequency regime but these tests are known to be prone to false positives. There is a more robust approach that can be formulated in the Bayesian framework. This approach assesses the probability that a mode is present, in contrast to the frequentist approach that tests that the data are consistent with being pure noise. In addition to being more robust, our Bayesian formulation allows us to bring to bear the strong a priori information that can be extrapolated from easy to detect modes. Here we have searched both smoothed and unsmoothed power spectra for modes using the Bayesian statistics described in Appourchaux, Samadi & Dupret (2009) as well as in Broomhall et al. (2010). For the rest of this paper we use modes that were detected by the Bayesian method and in the following section estimate their intrinsic properties.

2.3 Mode parameter estimation

Parameter estimation of modes detected in the previous section was performed using a Markov chain Monte Carlo (MCMC) fitting code. In this section we will first define the model used to describe the data, then the likelihood function, and finally discuss the actual fitting process.

2.3.1 Power spectrum model

Acoustic modes of oscillation are considered as stochastically excited and intrinsically damped harmonic oscillators. Consequently, the observed structure in the power spectrum due to a single mode is a Lorentzian profile multiplied by the χ^2 2 degrees-of-freedom forcing function (Anderson, Duvall & Jefferies 1990). In fact, there are additional contributions to the χ^2_2 function from the background but here we will constrain ourselves to considering only the mode of oscillation. The limit spectrum (at the limit of infinite observation) for a given degree (l) and radial order (n) is described by a Lorentzian profile with height $h_{n,\,l}$, width $w_{n,\,l}$, truncated asymmetry (Fletcher et al. 2009b) $b_{n,\,l}$, and central frequency $\nu_{n,\,l}$. Hence the model for a single mode of oscillation, $M(\nu)$, is

$$M_{n,l}(\nu) = \frac{h_{n,l}(1 + 2b_{n,l}x)}{1 + x^2}, \tag{4}$$

where

$$x = \frac{2}{w_{n,l}}\left(\nu - \nu_{n,l}\right). \tag{5}$$

The inclusion of rotation lifts the degeneracy of non-radial modes so that the frequency of a split component is dependent on azimuthal order, m. Modes are rotationally split into $2l + 1$ components with the splitting distance in frequency, $m\,\delta\nu_{n,\,l}$, determined to first order only by the weighted mean of the solar rotation rate. This assumption of equidistant splitting ignores the negligible effects in the Sun of centrifugal distortion (Ballot 2010), differential rotation effects which at solar magnitudes are virtually indistinguishable from solid body rotation, and asymmetries in the splitting caused by near surface magnetic fields, which again are very difficult to detect even at high signal-to-noise ratios (see Gough & Thompson 1990; Chaplin 2011). So the rotationally split frequencies may be written simply as

$$\nu_{n,l,m} = \nu_{n,l} + m\,\delta\nu_{n,l}. \tag{6}$$

In reality, the height, width, and asymmetry are dependent upon the azimuthal order. Here we make the assumption that mode width and asymmetry are defined by their position in frequency in the corotating frame of reference. We have assumed that inertial forces are negligible and consider the intrinsic properties of the rotationally split modes to be the same. Hence, we define the azimuthal components of the same mode to have a single width and asymmetry, i.e. $w_{n,\,l,\,m} = w_{n,\,l}$ and $b_{n,\,l,\,m} = b_{n,\,l}$. Furthermore, the height parameter is in principle determined only by the geometry of the degree and azimuthal order. However, the nature of the ground-based BiSON observations analysed here introduces significant departure from the theoretical azimuthal visibility. One could estimate the relative $h_{n,\,l,\,m}$ given enough information about the temporally averaged disc weighting from the terrestrial atmosphere and optical depth effects in the BiSON instrument (Christensen-Dalsgaard 1989). However, Chaplin et al. (1996) have shown that their best estimated are significantly different from those observed so here we determine the relative heights of $h_{n,\,l,\,m}$ empirically.

To determine the empirical factors $h_{n,\,l,\,m}$ we re-parametrize in terms of the mode height ($h_{n,\,l}$) and the correction dependent on degree and azimuthal order ($\epsilon_{l,\,m}$). We define

$$h_{n,l,m} = h_{n,l}\epsilon_{l,m}. \tag{7}$$

In this formulation we set the sectoral correction, $\epsilon_{l,\,m\,=\,l}$, to a value of unity thus keeping $h_{n,\,l}$ and $\epsilon_{l,\,m}$ as independent parameters. In addition, energy equipartition is expected between components of the same $|m|$ if the length of observation time-scale is greater than a few mode lifetimes (this is valid for lowest frequency non-radial mode reported in this study). This simplification allows us to constrain the parameter space by setting $\epsilon_{l,\,m} = \epsilon_{l,\,-m}$.

Furthermore, we will ignore the small contribution from azimuthal components where $l - m$ is odd. The solar angular momentum vector lies almost but not perfectly in the projected plane of the sky and so only components with even $l - m$ are observed (Chaplin et al. 2013). There is some small contribution[1] from the odd $l - m$ components generated by the non-zero solar tilt angle, but this effect has not been detected with significance for BiSON data in the best signal-to-noise ratio regions.

We have constrained $\epsilon_{l,\,|m|}$ for $l \leq 3$ for all but two combinations: $l = 2, m = 0$, and $l = 3, m = 1$. These two values must be determined by the fitting process. We can then modify equation (4) to include our prescription for rotational splitting:

$$M_{n,l}(\nu) = \sum_{m=-l}^{l} \frac{\epsilon_{l,|m|}\,h_{n,l}(1 + 2b_{n,l}x)}{1 + x^2}, \tag{8}$$

where x is now defined as

$$x = \frac{2}{w_{n,l}}\left(\nu - \nu_{n,l} - m\,\delta\nu_{n,l}\right). \tag{9}$$

The chosen BiSON data set, collected by a ground-based global network of telescopes, is subject to interruption from bad weather and occasional equipment malfunction. This reduction in duty cycle is known to impact the observed power spectrum (see earlier, Fletcher et al. 2009a, 2011) and hence the limit spectrum will be modified. To compensate for this we convolve the proposed model with the window function in the frequency domain. Adding a white noise background (B) to the mode and applying the window function convolution gives our final model,

$$M^{\rm obs}(\nu) = \left[\sum_{m=-l}^{l} \frac{\epsilon_{l,|m|}\,h_{n,l}(1 + 2b_{n,l}x)}{1 + x^2} + B\right] W(\nu). \tag{10}$$

As is clear from the model, we assume that the range in frequency over which we assess the background is sufficiently narrow that the background is well described by a DC term, i.e. that the rate of change of the local background is small in our narrow region. This assumption is just valid at around 2 mHz, where the tails of nearby strong modes introduce a small gradient, but become increasingly valid at low-frequency as a result of increasing narrowness and small amplitude in the nearby modes.

While we fit the parameter of mode height, the intrinsic parameter of interest is actually the mode amplitude squared (V^2), otherwise known as the mode power. The definition of mode height we have chosen, that the reported height is that of the $|m| = l$ components,

[1] The solar tilt angle varies between approximately $+7\overset{\circ}{.}25$ and $-7\overset{\circ}{.}25$. If we assume the time averaged tilt angle is $3\overset{\circ}{.}625$ and consider only the geometric arguments then we have $\epsilon_{1,\,0} = 0.008$, $\epsilon_{2,\,1} = 0.016$, $\epsilon_{3,\,2} = 0.024$, and $\epsilon_{3,\,0} = 0.029$.

means we must compensate for all components when calculating the mode power. Hence the definition of the mode power is

$$V_{n,l}^2 = \frac{\pi h_{n,l} w_{n,l}}{2} \sum_{m=-l}^{l} \epsilon_{l,|m|}. \quad (11)$$

We move on to discuss the assessment of the likelihood function.

2.3.2 *Likelihood function*

In order to perform the MCMC integration over the parameter space we must define a likelihood function. We know the noise in the power spectrum is distributed as χ_2^2. As a result, Anderson et al. (1990) have shown that the negative log likelihood function for model M, with parameters θ, and observation O is

$$-\ln(L) = \sum_i \left\{ \ln\left(M_i(\theta)\right) + \frac{O_i}{M_i(\theta)} \right\}, \quad (12)$$

where i describes the frequency bin. Maximizing the likelihood is equivalent to minimizing the negative log likelihood.

Following from Bayes' theorem for a model assumed to be true, we can state that the posterior probability, $p(\theta|O, I)$, is proportional to the likelihood function, $L(O|\theta)$, multiplied by a prior probability function $p(\theta|I)$, where I is the prior information,

$$p(\theta|O, I) \propto L(O|\theta) p(\theta|I). \quad (13)$$

When we fit a model to a peak in the power spectrum we work with the negative logarithm of the likelihood, so transforming and disregarding the constant term (the ignored term, the global likelihood, is treated as constant because we have assumed our model to be true) gives

$$-\ln[p(\theta|O, I)] = -\ln[L(O|\theta)] - \ln[p(\theta|I)]. \quad (14)$$

We wish to determine the probability density distributions of the parameters given the observations and the prior probability.

2.3.3 *Parameter estimation algorithm*

In this work, parameter estimation is achieved using a standard flavour of MCMC – the Metropolis algorithm (Metropolis et al. 1953). In brief, MCMC is a method based on drawing values of θ from proposal distributions and then correcting those draws to better approximate the target posterior distribution. Specifically, the Metropolis algorithm is an adaptation of a random walk that uses an acceptance rule to converge to our desired distribution. Note that the ubiquitous Metropolis–Hastings algorithm, which allows asymmetric proposal distributions, is an extension to the basic Metropolis algorithm that requires symmetric proposal distributions.

In the low-frequency regime, where modes have narrow line widths, there is little sensitivity to mode asymmetry. One approach might be to set the mode asymmetry to zero or some other arbitrary value but we can do better. Mode asymmetry in the low-frequency regime is of some interest but the nature of the model, the intrinsic mode parameters, and the resulting sensitivity to asymmetry provide little to no constraint. A strength of Bayesian methods, here the MCMC method, is that we are able to account for our lack of constraint or knowledge in 'nuisance' parameters-like mode asymmetry. Our lack of a posteriori knowledge of mode asymmetry is accounted for in the marginalized posterior probability distributions (PPDs) for our parameters of interest. Put more simply, the possible values of mode asymmetry are considered in the estimates of other parameters and when asymmetry is correlated with another parameter (for example mode frequency) the measured PPDs are slightly wider. This increase in uncertainty is real and it is right that we account for it.

The background model we apply is that of a flat local background which does not represent a physical model but we consider this to be reasonable when assessed over a narrow range in frequency. As is defined by our model we fit on a mode-by-mode basis, i.e. we consider only one mode at a time. This allows us to define a single parameter to describe the background. In reality, the background is made up of at least three contributions: solar granulation, stochastic noise, and the Lorentzian tails of nearby modes. As with mode asymmetry, marginalization propagates the uncertainty in the background value into the mode parameters of interest. However, we do note that because we assume our model to be true, this propagation of uncertainty only applies for the chosen model.

Mode parameters vary with the solar cycle but for low-frequency modes the variation is essentially undetectable because mode cavities do not (strongly) overlap radially with the source of the variation (Basu et al. 2012). We cannot study the solar cycle variation of the low signal-to-noise ratio low-frequency modes using short time series as the signal from these modes drops into the noise. As a result we are forced to measure the time averaged properties of the modes. Broomhall et al. (2009) proposed a correction to raw frequencies to recover frequencies pertinent to a quiescent Sun but this correction has to be extrapolated to frequencies lower than 1.5 mHz. The extrapolation suggests that any correction is of a similar magnitude to the uncertainties found here. Hence, the results we report are the raw fitted parameters uncorrected for the effects of the solar cycle.

3 RESULTS

Table 1 gives the median values together with the 67 per cent confidence intervals for frequency, line width, height, amplitude squared, and rotational splitting for BiSON modes at low frequency using the fitting analysis described above. For the first time we detect the low-frequency mode $n = 7, l = 0$ and both components of the sectoral multiplet structure of the $n = 7, l = 1$ mode. In addition we provide many previously unpublished values of mode height, line width, amplitude, and rotational splitting, all produced from a robust and homogeneous analysis. The marginalized PPDs for width, height, and amplitude are log-normal distributions so here we report the descriptive statistics, the median and 67 per cent confidence intervals, for the natural log of these parameters.

3.1 Mode line width and height

Fig. 3 shows mode line width as a function of mode frequency. A power law fitted to the widths of the modes whose frequencies are below 1.7 mHz is shown to approximate the variation of w with respect to the mode frequency at low frequency. It should be noted that this is not a good approximation at all frequencies and that the gradient/exponent returned from the fit is sensitive to the maximum mode frequency considered. Here we have ignored modes with frequencies above 1.7 mHz which provides a balance between minimizing the impact of the flattening of the curve at higher frequencies but still maintaining enough points for good constraint.

We do not suggest that the returned exponent (or offset) is a robust measure – the values of line width for each mode are the parameters any further study should use. Having said that, historically it is this exponent that has been the focus of discussion. The result

Table 1. Results from fitting to modes detected in the power spectra. Quoted errors are the 67 per cent confidence intervals.

n	l	Frequency (μHz)	Ln width (μHz)	Ln height ($m^2\,s^{-2}\,\mu Hz^{-1}$)	Ln amplitude^2 ($m^2\,s^{-2}$)	Splitting (μHz)
6	0	$972.615^{+0.002}_{-0.002}$	$-5.2^{+0.8}_{-0.6}$	$5.8^{+0.9}_{-0.9}$	$1.2^{+0.4}_{-0.4}$	–
7	0	$1117.993^{+0.004}_{-0.004}$	$-4.7^{+0.5}_{-0.4}$	$5.3^{+0.5}_{-0.4}$	$1.0^{+0.4}_{-0.4}$	–
7	1	$1185.604^{+0.003}_{-0.003}$	$-4.7^{+0.6}_{-1.2}$	$5.4^{+1.6}_{-0.5}$	$2.0^{+0.3}_{-0.3}$	$0.402^{+0.003}_{-0.003}$
8	0	$1263.198^{+0.005}_{-0.005}$	$-3.8^{+0.6}_{-1.5}$	$5.3^{+1.8}_{-0.5}$	$2.0^{+0.3}_{-0.3}$	–
8	1	$1329.635^{+0.003}_{-0.003}$	$-3.8^{+0.3}_{-0.2}$	$5.5^{+0.3}_{-0.3}$	$2.8^{+0.2}_{-0.2}$	$0.397^{+0.003}_{-0.003}$
8	2	$1394.689^{+0.005}_{-0.005}$	$-3.5^{+0.3}_{-0.3}$	$4.6^{+0.3}_{-0.3}$	$2.5^{+0.2}_{-0.2}$	$0.405^{+0.002}_{-0.002}$
9	0	$1407.472^{+0.006}_{-0.006}$	$-3.4^{+0.4}_{-0.4}$	$5.3^{+0.4}_{-0.4}$	$2.4^{+0.2}_{-0.2}$	–
9	1	$1472.839^{+0.006}_{-0.006}$	$-2.5^{+0.2}_{-0.2}$	$4.9^{+0.2}_{-0.2}$	$3.5^{+0.1}_{-0.1}$	$0.398^{+0.005}_{-0.005}$
9	2	$1535.853^{+0.005}_{-0.005}$	$-2.6^{+0.2}_{-0.1}$	$5.0^{+0.2}_{-0.2}$	$3.7^{+0.1}_{-0.1}$	$0.407^{+0.003}_{-0.003}$
10	0	$1548.336^{+0.007}_{-0.007}$	$-2.5^{+0.2}_{-0.2}$	$5.4^{+0.2}_{-0.2}$	$3.4^{+0.1}_{-0.1}$	–
9	3	$1591.536^{+0.014}_{-0.014}$	$-2.4^{+0.3}_{-0.3}$	$3.7^{+0.3}_{-0.3}$	$2.77^{+0.2}_{-0.2}$	$0.400^{+0.005}_{-0.005}$
10	1	$1612.724^{+0.006}_{-0.006}$	$-2.2^{+0.2}_{-0.1}$	$5.6^{+0.1}_{-0.2}$	$4.56^{+0.06}_{-0.06}$	$0.404^{+0.005}_{-0.005}$
10	2	$1674.538^{+0.008}_{-0.008}$	$-1.8^{+0.1}_{-0.1}$	$4.9^{+0.1}_{-0.1}$	$4.55^{+0.06}_{-0.06}$	$0.402^{+0.004}_{-0.004}$
11	0	$1686.594^{+0.012}_{-0.012}$	$-1.6^{+0.1}_{-0.1}$	$5.3^{+0.1}_{-0.1}$	$4.18^{+0.08}_{-0.08}$	–
10	3	$1729.088^{+0.022}_{-0.022}$	$-1.4^{+0.2}_{-0.2}$	$3.5^{+0.2}_{-0.2}$	$3.65^{+0.12}_{-0.12}$	–
11	1	$1749.285^{+0.007}_{-0.007}$	$-1.7^{+0.1}_{-0.1}$	$5.8^{+0.1}_{-0.1}$	$5.26^{+0.05}_{-0.05}$	$0.407^{+0.008}_{-0.008}$
11	2	$1810.308^{+0.009}_{-0.009}$	$-1.3^{+0.1}_{-0.1}$	$5.2^{+0.1}_{-0.1}$	$5.28^{+0.04}_{-0.04}$	$0.403^{+0.004}_{-0.004}$
12	0	$1822.202^{+0.012}_{-0.012}$	$-1.2^{+0.1}_{-0.1}$	$5.8^{+0.1}_{-0.1}$	$5.04^{+0.05}_{-0.05}$	–
11	3	$1865.280^{+0.016}_{-0.016}$	$-1.0^{+0.1}_{-0.1}$	$4.2^{+0.1}_{-0.1}$	$4.66^{+0.06}_{-0.06}$	$0.395^{+0.005}_{-0.005}$
12	1	$1885.089^{+0.009}_{-0.009}$	$-1.1^{+<0.1}_{-<0.1}$	$6.0^{+<0.1}_{-<0.1}$	$6.03^{+0.03}_{-0.03}$	$0.403^{+0.008}_{-0.008}$
12	2	$1945.824^{+0.013}_{-0.013}$	$-0.8^{+<0.1}_{-<0.1}$	$5.4^{+<0.1}_{-<0.1}$	$5.99^{+0.03}_{-0.03}$	$0.392^{+0.006}_{-0.006}$
13	0	$1957.452^{+0.012}_{-0.012}$	$-0.9^{+<0.1}_{-<0.1}$	$6.1^{+0.1}_{-0.1}$	$5.66^{+0.04}_{-0.04}$	–

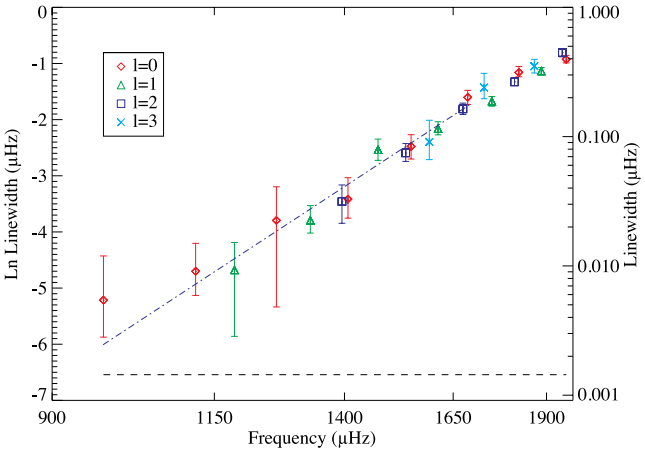

Figure 3. Mode line widths as a function of frequency from fitting to the BiSON power spectrum, plotted in ln–ln space. The dashed horizontal line is the frequency resolution, i.e. the bin width.

we report here is $\alpha = 7.9 \pm 0.6$ which is consistent, albeit with smaller uncertainty, with observations by Chaplin et al. (1997b) ($\alpha = 7.0 \pm 1.5$) and Roca Cortés et al. (1999) ($\alpha = 8.2 \pm 1.5$), and in agreement with theory from Balmforth (1992) and Goldreich, Murray & Kumar (1994) ($\alpha = 8.0$).

3.2 Mode amplitude

Fig. 4 shows the mode amplitude squared (or mode power) as a function of mode frequency. Fits to the data have been performed separately for $l = 0, 1$, and 2. Again the fits performed to the observations match a power law in frequency. Again we reiterate that the robust results here are the individual amplitudes not the fits made

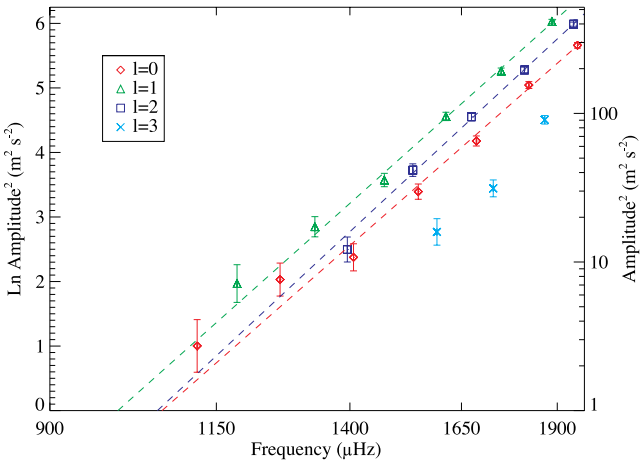

Figure 4. Mode amplitudes squared as a function of frequency from fitting to the BiSON power spectrum, plotted in ln-ln space.

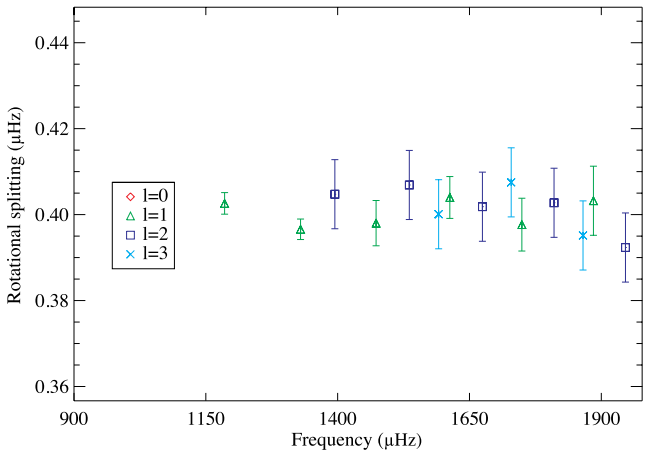

Figure 5. Mode rotational splitting as a function of frequency from fitting to the BiSON power spectrum, plotted in ln-linear space.

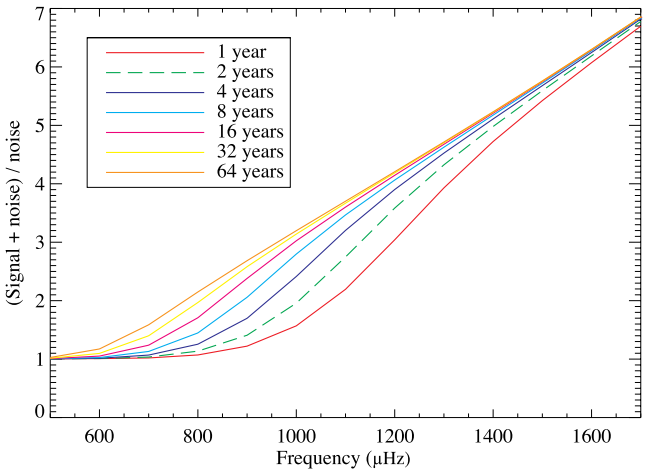

Figure 6. Radial mode detectability at low frequency, for different length of observation, extrapolated from measurements presented in this paper.

to these data. We make the fits only for the purpose of allowing the study of mode detectability at low frequency – the focus of a later section.

3.3 Mode rotational splitting

Fig. 5 shows the measured mode rotational splitting as a function of mode frequency. The results show no significant gradient with frequency. We fitted a linear model to the splitting as a function of frequency. In addition, fitting a higher order polynomial provides no statistically significant improvement when accounting for the additional model complexity. Hence we conclude that we see no significant variation in rotational splitting as a function of frequency.

3.4 Mode detectability at low frequency

The detectability of a mode in a very long time series is dependent on the mode amplitude, the mode line width, and the length of observation (T). We have estimated the frequency dependency of line width and amplitude and here combine this with the length of time series to estimate a maximum height in the limit spectrum.

The observed height of a frequency bin is defined by the limit spectrum multiplied by the noise function. Here we remove the stochastic nature of modes of oscillation and consider only the limit spectrum. From earlier, the limit spectrum ($Y(\nu)$) is the convolution of the signal ($S(\nu)$) with the window function $W(\nu)$,

$$Y(\nu) = S(\nu)W(\nu). \tag{15}$$

Here we define the signal as a radial mode of oscillation:

$$S^{\rm sym}(\nu) = \frac{h}{1 + \frac{4}{w^2}(\nu - \nu_{\rm c})^2}, \tag{16}$$

where $\nu_{\rm c}$ is the central frequency of the mode. To determine the height and width we use the power-law relations ($V^2(\nu)$ and $w(\nu)$) determined in this paper assessed at $\nu_{\rm c}$ where,

$$h(\nu_{\rm c}) = \frac{2\,V^2(\nu_{\rm c})}{\pi w(\nu_{\rm c})}. \tag{17}$$

The window function of a continuous but finite observation is a sinc^2 function with width equal to the spectral resolution,

$$W(\nu) = 2T\,{\rm sinc}^2(2\pi T\nu). \tag{18}$$

The maximum bin height (Z) will be realized when the $\nu_{\rm c}$ is equal to the bin frequency (ν). We can then, for a given T, determine Z at a range of mode central frequencies,

$$Z(\nu_{\rm c}; T) = P(\nu = \nu_{\rm c}; T). \tag{19}$$

The required convolution is computed numerically in the frequency domain giving us the ability to calculate $Z(\nu_{\rm c}; T)$ at a range of mode frequencies and for different lengths of observation.

Fig. 6 shows the calculated height of the signal but in terms of the mode detectability, which is much better characterized by the signal plus the background divided by the background, $(Z + B)/B$. Here we use the BiSON 22 yr background scaled as power per Hz to provide something that is comparable to the background that might be measured for time series of different lengths.

Fig. 6 demonstrates why the detection limit of low-frequency p modes has remained around 1 mHz for the last decade. A combination of the intrinsic mode properties and the noise conspire to obscure the low-frequency p modes below the current limits. Performing nothing more than continued observation does not significantly reduce these limits. Detections may be possible below the current limits with better or novel treatments of the background noise or unusually large mode excitations. It is possible that combinations of observations can be constructed that share coherent signal yet incoherent backgrounds, for example observing at varying height in the solar atmosphere. However, the possibility of observing modes below 950 μHz appears to be a significant observational challenge.

4 CONCLUSIONS

This paper presents the measured the properties of the low-frequency p modes as observed by BiSON over 22 yr including new mode detections. We have detected and characterized the previously unpublished $l = 0$, $n = 7$ mode at ≈1118 μHz and have unambiguously detected both of the sectoral components ($m = \pm 1$) for the $l = 1$, $n = 7$ mode at ≈1186 μHz. These frequencies can be used in detailed helioseismic modelling and should be particularly prized for their very small uncertainties.

We have reported new and robust values of rotational splitting which may be used in rotational inversions. The error bars on the lowest frequency rotational splitting again provide the potential for new constraint and inference. In addition, we have reported new

values of mode height, line width, and amplitude that will provide diagnostics on the poorly understood near-surface convection.

The analysis provided is a demonstration of cutting-edge helioseismic peak-bagging techniques. Each reported mode has been detected using robust Bayesian detection statistics and then further analysed to determine robust mode characteristics by estimating the posterior probability density function for each parameter. The use of MCMC methods, instead of maximum likelihood estimates plus formal error estimates through the inverse Hessian matrix (which are lower limits on the uncertainty), provides accurate 67 per cent confidence intervals for all parameters. Using these values we have fitted a simple power law to the mode line width to allow for comparison with previous studies and extrapolation at lower frequency. For the mode line width dependence with respect to frequency we find good agreement between previous studies. Our uncertainty on the exponent is significantly smaller than those quoted previously, and is in good agreement with theoretical values.

We put forward a justification for the apparent difficulty in extending the frequency range for which low-frequency modes are detected. The data presented allow us to introduce a parametrization of the mode characterization which permits the prediction of the signal-to-noise ratio at frequencies below the detection threshold. We have shown that the intrinsic properties of the low-frequency p modes make further detections at frequencies below 950 μHz a real observational challenge. Our analysis tells us that the best approach to extending the low-frequency range is to develop a method to overcome the low-frequency noise due to solar granulation or instrumental effects *and* to observe for an extended period of time.

ACKNOWLEDGEMENTS

We would like to thank all those who are, or have been, associated with BiSON. AMB thanks the Institute of Advanced Study, University of Warwick, for their support. BiSON is funded by the Science and Technology Facilities Council (STFC). We acknowledge the Leverhulme Trust for funding the 'Probing the Sun: inside and out' project upon which this research is based.

REFERENCES

Anderson E. R., Duvall T. L., Jr, Jefferies S. M., 1990, ApJ, 364, 699
Appourchaux T., 2011, preprint (arXiv:e-prints)
Appourchaux T., Samadi R., Dupret M.-A., 2009, A&A, 506, 1
Appourchaux T. et al., 2010, A&AR, 18, 197
Appourchaux T. et al., 2012, A&A, 543, A54
Ballot J., 2010, Astron. Nachr., 331, 933
Balmforth N. J., 1992, MNRAS, 255, 639
Basu S., Broomhall A.-M., Chaplin W. J., Elsworth Y., 2012, ApJ, 758, 43
Brookes J. R., Isaak G. R., van der Raay H. B., 1978, MNRAS, 185, 1
Broomhall A. M., Chaplin W. J., Elsworth Y., Appourchaux T., 2007, MNRAS, 379, 2
Broomhall A.-M., Chaplin W. J., Elsworth Y., Fletcher S. T., New R., 2009, A&A, 503, 241
Broomhall A.-M., Chaplin W. J., Elsworth Y., Appourchaux T., New R., 2010, MNRAS, 406, 767
Chaplin W. J., 2011, preprint (arXiv:e-prints)
Chaplin W. J., Elsworth Y., Howe R., Isaak G. R., McLeod C. P., Miller B. A., New R., 1996, MNRAS, 280, 1162
Chaplin W. J., Elsworth Y., Howe R., Isaak G. R., McLeod C. P., Miller B. A., New R., 1997a, A&AS, 125, 195
Chaplin W. J., Elsworth Y., Isaak G. R., McLeod C. P., Miller B. A., New R., 1997b, MNRAS, 288, 623
Chaplin W. J., Elsworth Y., Isaak G. R., Lines R., McLeod C. P., Miller B. A., New R., 1998, MNRAS, 298, L7
Chaplin W. J., Elsworth Y., Isaak G. R., Marchenkov K. I., Miller B. A., New R., 2001, MNRAS, 327, 1127
Chaplin W. J., Elsworth Y., Isaak G. R., Miller B. A., New R., 2002, MNRAS, 330, 731
Chaplin W. J., Elsworth Y., Isaak G. R., Miller B. A., New R., Pintér B., 2003, in Sawaya-Lacoste H., ed., Proceedings of SOHO 12/GONG+ 2002, Local and Global Helioseismology: The Present and Future, ESA SP-517. ESA, Noordwijk, p. 183
Chaplin W. J. et al., 2013, ApJ, 766, 101
Christensen-Dalsgaard J., 1989, MNRAS, 239, 977
Elsworth Y., Howe R., Isaak G. R., McLeod C. P., Miller B. A., New R., Wheeler S. J., 1995, A&AS, 113, 379
Fletcher S., New R., Chaplin W., Elsworth Y., 2009a, in Dikpati M., Arentoft T., González Hernández I., Lindsey C., Hill F., eds, ASP Conf. Ser. Vol. 416, Solar–Stellar Dynamos as Revealed by Helio- and Asteroseismology: GONG 2008/SOHO 21. Astron. Soc. Pac., San Francisco, p. 519
Fletcher S. T., Chaplin W. J., Elsworth Y., New R., 2009b, ApJ, 694, 144
Fletcher S. T., Broomhall A.-M., Chaplin W. J., Elsworth Y., New R., 2011, MNRAS, 415, 1310
Garcia R. A. et al., 2001, Sol. Phys., 200, 361
García R. A., Turck-Chièze S., Jiménez-Reyes S. J., Ballot J., Pallé P. L., Eff-Darwich A., Mathur S., Provost J., 2007, Science, 316, 1591
Goldreich P., Murray N., Kumar P., 1994, ApJ, 424, 466
Gough D. O., Thompson M. J., 1990, MNRAS, 242, 25
Houdek G., Balmforth N. J., Christensen-Dalsgaard J., Gough D. O., 1999, A&A, 351, 582
Lazrek M., Hill F., 1993, A&A, 280, 704
Metropolis N., Rosenbluth A. W., Rosenbluth M. N., Teller A. H., Teller E., 1953, J. Chem. Phys., 21, 1087
Roca Cortés T., Montañés P., Pallé P. L., Pérez Hernández F., Jiménez A., Régulo C. The GOLF Team, 1999, in Gimenez A., Guinan E. F., Montesinos B., eds, ASP Conf. Ser. Vol. 173, Stellar Structure: Theory and Test of Connective Energy Transport. Astron. Soc. Pac., San Francisco, p. 305
Thompson M. J., Christensen-Dalsgaard J., Miesch M. S., Toomre J., 2003, ARA&A, 41, 599

This paper has been typeset from a TEX/LATEX file prepared by the author.